Applied Radiation and Isotopes 85 (2014) 39–44

Contents lists available at ScienceDirect

Applied Radiation and Isotopes

journal homepage: www.elsevier.com/locate/apradiso

Production of medical radioisotopes with linear accelerators

Valeriia N. Starovoitova *, Lali Tchelidze [1], Douglas P. Wells [2]

Idaho State University, Idaho Accelerator Center, 1500 Alvin Ricken Dr, Pocatello, ID 83201, United States

HIGHLIGHTS

- We simulated ^{99}Mo and ^{67}Cu yield using photonuclear reactions ^{100}Mo(γ,n)^{99}Mo and ^{68}Zn(γ,p)^{67}Cu.
- We verified the predicted activities with experimental data.
- We propose a separation scheme, based on kinematic recoil, for isotopes produced via photoneutron method.
- The efficiency of this separation scheme was simulated for ^{100}Mo(γ,n)^{99}Mo example.

ARTICLE INFO

Article history:
Received 22 February 2013
Received in revised form
21 July 2013
Accepted 29 November 2013
Available online 11 December 2013

Keywords:
Radioisotopes
Electron accelerators
Photonuclear production

ABSTRACT

In this study, we discuss producing radioisotopes using linear electron accelerators and address production and separation issues of photoneutron (γ,n) and photoproton (γ,p) reactions. While (γ,n) reactions typically result in greater yields, separating product nuclides from the target is challenging since the chemical properties of both are the same. Yields of (γ,p) reactions are typically lower than (γ,n) ones, however they have the advantage that target and product nuclides belong to different chemical species so their separation is often not such an intricate problem. In this paper we consider two examples, ^{100}Mo(γ,n)^{99}Mo and ^{68}Zn(γ,p)^{67}Cu, of photonuclear reactions. Monte-Carlo simulations of the yields are benchmarked with experimental data obtained at the Idaho Accelerator Center using a 44 MeV linear electron accelerator. We propose using a kinematic recoil method for photoneutron production. This technique requires ^{100}Mo target material to be in the form of nanoparticles coated with a catcher material. During irradiation, ^{99}Mo atoms recoil and get trapped in the coating layer. After irradiation, the coating is dissolved and ^{99}Mo is collected. At the same time, ^{100}Mo nanoparticles can be reused. For the photoproduction method, ^{67}Cu can be separated from the target nuclides, ^{68}Zn, using standard exchange chromatography methods. Monte-Carlo simulations were performed and the ^{99}Mo activity was predicted to be about 7 MBq/(g*kW*h) while ^{67}Cu activity was predicted to be about 1 MBq/(g*kW*h). Experimental data confirm the predicted activity for both cases which proves that photonuclear reactions can be used to produce radioisotopes. Lists of medical isotopes which might be obtained using photonuclear reactions have been compiled and are included as well.

1. Introduction

Radioisotopes have a wide variety of uses in industry, science, and medicine. Nuclear medicine is the most demanding consumer of radioisotopes. In particular, radioisotopes are used for medical product sterilization, cardiac diagnostic procedures, bone and tumor scans, and radioisotope therapy. The nation's inventory of many radio-isotopes rely on too few facilities to provide adequate quantity and reliability of the supply. Steady production of currently used isotopes and creation of new isotopes for medical research would enable further advances in nuclear medicine and biomedical sciences.

Currently the majority of medical isotopes are produced in either reactors or cyclotrons. In general, neutron-rich radioisotopes, such as $^{99\,m}$Tc, ^{60}Co, ^{192}Ir, ^{131}I, ^{166}Ho, ^{177}Lu, are produced in reactors either as fission products or via neutron capture and have relatively longer half-lives, etc. (Han et al., 2003; Ball, 2003; Knapp (Russ) et al., 2005; Bokhari and Mushtaq (2010); Mikolajczak et al., 2003). On the other hand, neutron-deficient radioisotopes, such as ^{18}F, ^{201}Tl, ^{123}I, ^{67}Ga, are typically produced in cyclotrons via (p,xn) and (p,α) reactions and have relatively short half-lives (Sajjad and Lambrecht, 1993; Le Bars, 2006; Haddad et al., 2008; Kim et al., 2009).

Until recently an almost uninterrupted supply of many cheap, subsidized reactor produced isotopes, such as ^{99}Mo, existed. However, recent supply disruptions led to serious discussions on how to secure the supply of such radiopharmaceuticals in the future. To compound the current situation, most of the current reactors-producing radioisotopes are scheduled to be taken offline in the next few years. Even though historically reactor-based

* Corresponding author. Tel.: +1 208 282 5254; fax: +1 208 282 5878.
E-mail address: starvale@isu.edu (V.N. Starovoitova).
[1] Currently at European Spallation Source, Box 176, 22100 Lund, Sweden
[2] Currently at South Dakota School of Mines and Technology, 501 East Saint Joseph St, Rapid City, SD 57701, United States

0969-8043/$ - see front matter © 2013 Elsevier Ltd. All rights reserved.
http://dx.doi.org/10.1016/j.apradiso.2013.11.122

production schemes have been chosen over accelerator-based production schemes, the continued disruptions and scheduled shutdowns demonstrate that the reactor method is no longer reliable.

Accelerators, on the other hand, have a number of advantages over nuclear reactors for radioisotope production, such as safety and cheaper operating and decommissioning costs. Since accelerators are powered by electricity rather than fission reactions, they generate far less than 10% of the waste of research reactors. Furthermore, accelerator-produced waste is less hazardous than waste produced by a research reactor. Finally, accelerators do not pose a nuclear weapon proliferation risk.

Even though many isotopes are already being produced using proton accelerators (cyclotrons), linear electron accelerators (LINACs) are not widely used for isotope production yet. While in case of cyclotrons transmutations are proton-induced, in case of LINACs, electrons do not knock out nucleons directly. Instead, being incident on a converter they break and produce bremsstrahlung photons, which cause photo-nuclear processes. Typically, a high energy electron beam (20–40 MeV) is used to produce a cone of bremsstrahlung photons. Several feasibility studies have demonstrated the viability of linear electron accelerators to produce radioisotopes (Aizatsky et al., 2010; Danon et al., 2008; Maslov et al., 2006; Tchelidze, 2010; Starovoitova et al., 2010; KC et al., 2012). In this paper we will discuss the advantages and disadvantages of photoneutron and photoproton production of medical radioisotopes using electron accelerators.

2. Methods

Photonuclear reactions can be described as a two-stage process. During the first stage a photon is absorbed, and a nucleus becomes excited. For energies below about 10 MeV only narrow resonance peaks exist, corresponding to exciting a single nuclear level. In general the resonance lines are very sharp and thus even though the peak cross-section can reach thousands of barns, the integrated cross-section is very small. This energy region is not useful for the photonuclear production of isotopes. In the energy range from approximately 10 MeV to about 30 MeV a very broad resonance maximum is observed. This region, called giant dipole resonance (GDR), represents the collective vibrational motion of the neutrons against the protons inside the nucleus. This is the most suitable energy region for photonuclear production. If the photon energy exceeds about 30 MeV, it interacts with a correlated neutron–proton pair (deuteron) instead of collective excitation of all the nucleons. This leads to a single nucleon emission and results in a relatively low cross-section. Finally, photons with energies over 140 MeV can produce pi-mesons and thus the total photoabsorption cross-section rises again.

During the second stage, the excitation energy is released – in the form of a photon, neutron, or a charged particle (proton, alpha particle, etc). For the purpose of isotope production the most interesting cases are photoneutron and photoproton reactions, which are discussed below in detail.

2.1. Photoneutron production

The total cross section in the giant dipole resonance region is dominated by emission of a single nucleon (neutron or proton), even though elastic and inelastic scattering, emission of more than one nucleon and emission of composite charged particles (such as alpha) also plays a role. For medium and heavy nuclei emission of protons and other charged particles is lessen by the Coulomb barrier and the total photon absorption cross-section is almost completely given by the photoneutron cross-section. The simplest

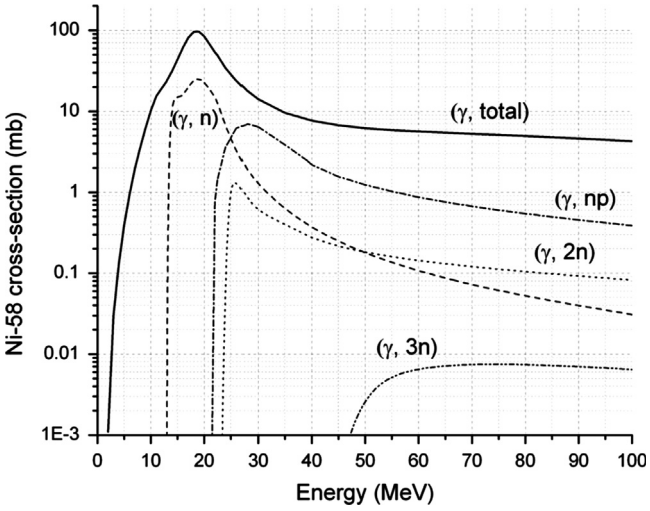

Fig. 1. Photoneutron cross-sections for Ni-58. Adopted from TENDL-2009 library.

Table 1
Threshold energies for different photoneutron reactions for Ni-58. Adopted from TENDL-2009 library.

Reaction	γ,n	γ,2n	γ,3n	γ,np
Threshold energy, MeV	13	24	40	20

photoneutron reaction is (γ,n), however, higher order reactions are also possible:

$$\sigma(\gamma, n_{total}) = \sigma(\gamma, n) + \sigma(\gamma, np) + \sigma(\gamma, 2n) + \sigma(\gamma, 2np) + \sigma(\gamma, 3n) + \ldots \quad (1)$$

The first term in this expression is dominant as can be seen in Fig. 1, however higher order terms start contributing as well once their threshold energy is reached (see Table 1). While providing relatively high yield, photoneutron production of most radioisotopes has a large drawback – low specific activity or activity per unit mass.

To increase the specific activity it is necessary to separate the daughter nuclide from the parent, which is the same chemical element, and generally this is a very difficult problem. To resolve this issue we suggest to employ nuclear kinematic recoil method.

Nuclear kinematic recoil has been studied for relatively long time (Cheng et al., 1999; Fujiwara et al., 1999; Haba et al., 1999). When a photon knocks a neutron out of the target nucleus, a photo-produced daughter nuclide recoils. The kinetic energy of some of those daughter nuclides is big enough to escape the bulk material and get trapped in the "catcher material" – another substance in contact with the target. As shown in Fig. 2, the recoiled atom gets trapped in the catcher particles. The smaller the size of the target particle is, the greater fraction of daughter particles is going to escape it and stop in the catcher particles. The production rate N' of the daughter particles is

$$N' = N_T \cdot I \quad (2)$$

where N_T is the number of atoms in the target and I is the photon flux – cross section overlap integral:

$$I = \int_{E_{th}}^{E_{max}} \varphi(E_\gamma) \cdot \sigma(E_\gamma) dE_\gamma \quad (3)$$

where $\sigma(E_\gamma)$ is the reaction cross-section and $\varphi(E_\gamma)$is the photon flux.

Using photonuclear cross-section and a Monte-Carlo simulated bremsstrahlung photon flux the integral I can be calculated and the daughter particles production rate N' can be estimated. Finally,

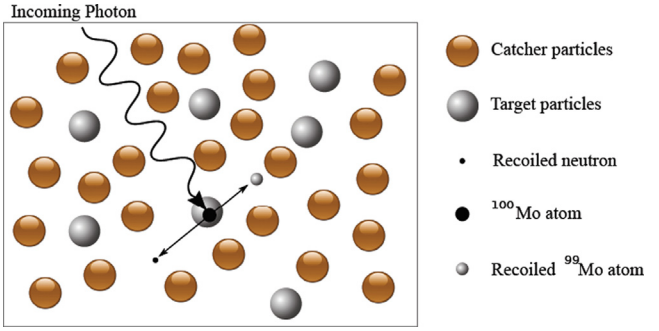

Fig. 2. The recoiled atom gets trapped in a catcher particles. The smaller the size of the target particles, the greater fraction of daughter nuclei is going to escape it and stop in the catcher particles.

the activity can be estimated after irradiation time of t_{irr} as

$$A = \lambda N = N' \cdot (1 - e^{-\lambda t_{irr}}) \quad (4)$$

where λ is the decay constant, and N is the number of product nuclei.

The range of a low energy ^{99}Mo atom (close to the peak energy of recoil spectrum) in natural molybdenum is several nm. That suggests that in order for the recoiled ^{99}Mo collection efficiency to be high, one needs to use nano-particles of molybdenum as targets. Depending on the size of a nano-particle, there is a certain fraction of produced ^{99}Mo ions escaping the particle and getting stopped in the particles of catcher material. This fraction drops as the target particle size increases. The smaller the target particle size is, the larger the escape fraction becomes. However, the ^{99}Mo ions, while traveling through the target, knock out stable molybdenum atoms, ^{100}Mo, some of which could also get out of the target particle and end up in the catcher. This obviously drops the value of the specific activity of ^{99}Mo in the catcher. Since our goal is to catch as much ^{99}Mo and as little ^{100}Mo as possible, we need a filter, or a barrier to let ^{99}Mo through and stop ^{100}Mo. Fortunately, energy distributions of ^{99}Mo and ^{100}Mo are quite different.

The energy spectrum of the daughter nuclides depends on the incident bremsstrahlung γ spectrum, target material, and cross section of the photonuclear reaction. The evaporation model for compound nuclei predicts that the emitted neutrons energy distribution approaches the form of a Maxwell distribution:

$$dN(E_n) \approx E_n e^{\left(\frac{E_n}{T}\right)} dE_n \quad (5)$$

where $dN(E_n)$ is the number of neutrons emitted with energy between E_n and $E_n + dE_n$ and T – with dimension of energy, has the role of a nuclear temperature. Using this equation the daughter nuclides recoil energy spectrum can be found and used to calculate their ranges in target material.

Stable ^{100}Mo atoms have a pronounced peak at low energies, while ^{99}Mo ions have more uniform distribution of energies. Thus if we coat a nano-particle with a thin layer of carbon, silicon-carbide, or aluminum, it will play a role of a barrier and will stop unwanted ^{100}Mo, but will let the majority of ^{99}Mo through. Potentially, we could coat the particles with another layer of the catcher material, so ^{99}Mo atoms will be collected into it. In this case, one would have to dissolve the outer layer after irradiation and collect ^{99}Mo. Molybdenum nano-particles with an inner coating layer we collected and re-coated with the outer layer before the next irradiation.

2.2. Photoproton production

Photoproton reactions are very similar to photoneutron ones. First, an incident photon is absorbed by the nuclei and causes it to be in an excited state. However, the de-excitation takes place via

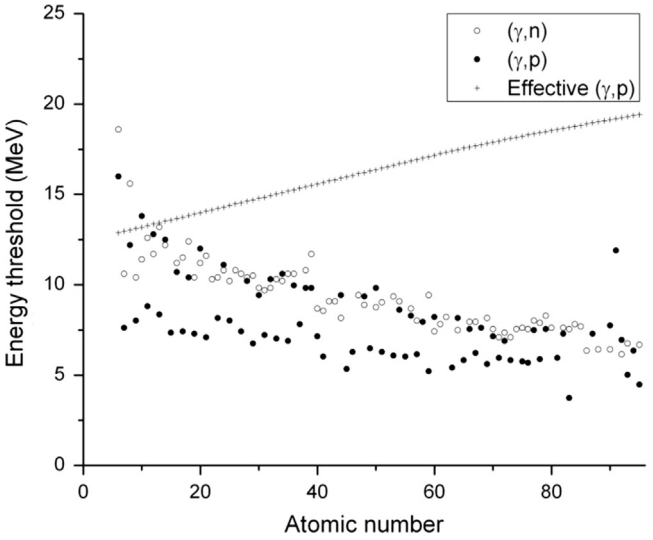

Fig. 3. Threshold energies of photonuclear reactions as a function of atomic number. Effective threshold is the threshold of (gamma, p) plus Coulomb barrier. Adopted from Segebade et al., 1987.

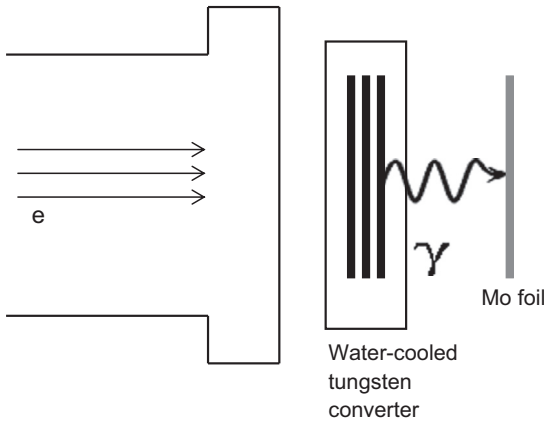

Fig. 4. Experimental setup. Electron beam is incident on the 4 mm thick tungsten converter. Mo foils are placed behind the converter.

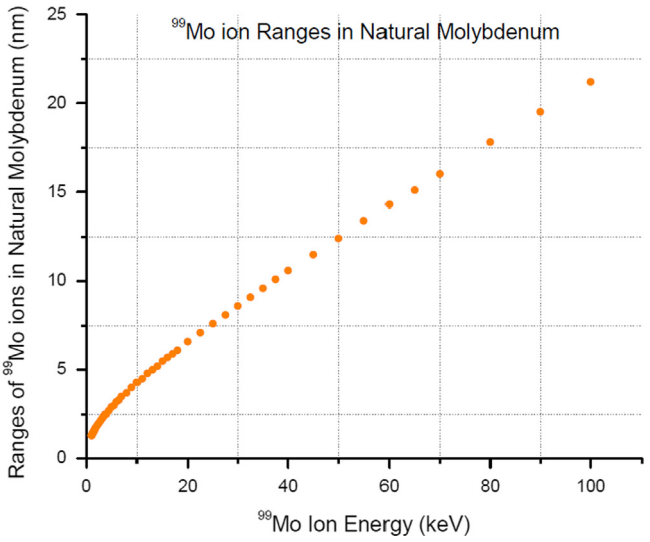

Fig. 5. ^{99}Mo ranges in natural molybdenum.

emitting one or more protons instead of neutrons. The emission of charged particles from an excited nucleus is hindered by the Coulomb barrier in addition to the nuclear forces. Once the photon energy is high enough to overcome the Coulomb barrier, the photoproton cross-section rises quickly. In general, (γ,p) reaction threshold energies are comparable to those of (γ,n) reactions, however, the effective (γ,p) thresholds, where the Coulomb potential is taken into consideration, are significantly higher. Also, the effective (γ,p) threshold, unlike the (γ,n) threshold, increases as Z increases (see Fig. 3). Due to the high effective threshold and the relatively low cross-section, photoproton production of radioisotopes is efficient only for light and medium elements.

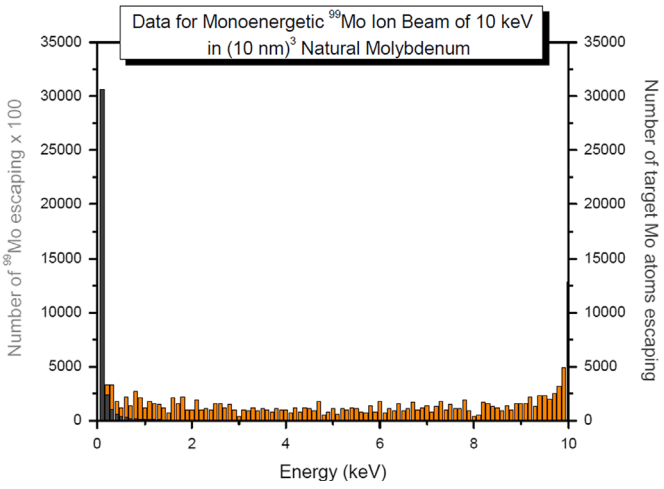

Fig. 6. Energy distribution for stable Mo and ^{99}Mo.

Table 2
Escape fractions for ^{99}Mo and ^{100}Mo obtained with SRIM software. 20 nm x 20 nm x 20 nm cube of natural molybdenum was assumed for the simulations. ^{99}Mo escape fraction, α, represents the ratio of the ^{99}Mo atoms escaping the target to the total number of ^{99}Mo atoms produced inside it. ^{100}Mo escape fraction, β, represents the ratio of the ^{100}Mo atoms escaping the target to the total number of ^{99}Mo atoms produced inside it.

Coating	^{99}Mo escape fraction, α	^{100}Mo escape fraction, β
None	0.56	26
Au, 2 nm	0.26	0.15
Au, 5 nm	0.09	0.01
Au, 10 nm	0.0018	0
Cu, 2 nm	0.29	0.14
Cu, 5 nm	0.1	0.014
Cu, 10 nm	0.017	0
Al, 2 nm	0.44	0.57
Al, 5 nm	0.29	0.1
Al, 10 nm	0.134	0.016
C, 5 nm	0.3	0.12
SiC, 5 nm	0.3	0.12

Photoproton reaction yields can be estimated using the same equation (Eq.4) as for photoneutron reactions. Even though in general the (γ,p) reaction yields are mediocre in comparison with (γ,n) ones, photoproton production has a huge advantage. Since (γ,p) reactions result in the daughter and the parent isotopes being chemically different species their separation is often trivial.

3. Results and discussion

3.1. Photoneutron reaction $^{100}Mo(\gamma,n)^{99}Mo$

To estimate the ^{99}Mo yield from the photoneutron reaction we have performed Monte-Carlo simulations of the photon flux. We assumed a 1 kW, 30 MeV electron beam, hitting a 4 mm thick tungsten converter and producing a cone of bremsstrahlung photons. We also assumed a 1 g target of natural molybdenum, placed right behind the converter. MCNPX (Monte-Carlo *N*-Particle Transport) software was used to predict the average photon flux through the target as a function of energy. This function was convoluted with a ^{100}Mo(γ,n)^{99}Mo reaction cross-section and a ^{99}Mo production rate was calculated to be $N' \approx 0.8 \times 10^8$ s^{-1}. Thus the ^{99}Mo activity after 15 h of irradiation would be about 1.1 × 10^7 Bq/(g*kW). The specific activity of the product would be low due to a large amount of ^{100}Mo in the sample. These simulations were benchmarked by experimental data collected at the Idaho Accelerator Center with a 44 MeV short pulsed linear electron accelerator. Natural molybdenum foils (typical mass was about 0.025 g) were placed after 4 mm thick water-cooled tungsten converter (see Fig. 4). Samples were irradiated for 1 h using 5 kW of electron beam power (280 Hz repetition rate, 250 mA peak current, 2.4 s pulse width and 30 MeV electron beam energy). ^{99}Mo activity was measured afterwards using gamma-spectroscopy. ^{99}Mo emits distinct gamma lines at 181 keV (6.2% branching ratio), 740 keV (12.8% branching ratio), and 778 keV

Table 3
Medical isotopes which can be obtained through the photoneutron production and their possible applications.

Nuclide	Half-life	Decay mode	Possible applications	Production
^{18}F	110 min	β^+	Radiotracer for brain studies, PET imaging	^{19}F (γ,n)^{18}F
^{47}Sc	3.35 d	β^-	Bone cancer pain relief, cancer radioimmunotherapy	^{48}Ca (γ,n)^{47}Ca ^{47}Ca (β^-)^{47}Sc
^{64}Cu	12.7 h	ε, β^-, β^+	SPECT imaging, cerebral and myocardial blood flow studies, colorectal cancer therapy	^{65}Cu (γ,n)^{64}Cu ^{66}Zn (γ,np)^{64}Cu
^{67}Ga	78.3 h	ε	Imaging of abdominal infections, detect Hodgkins/non-Hodgkins lymphoma, used with In-111 for soft tissue infections and osteomyelitis detection, evaluate sarcoidiodis and other granulomaous diseases, particularly in lungs and mediastiusim	^{69}Ga (γ,2n)^{67}Ga
^{75}Se	120 d	ε	Radiotracer used in brain studies, imaging of adrenal cortex by γ-scintigraphy, lateral locations of steroid secreting tumors, pancreatic scanning, detection of hyperactive parathyroid glands	^{76}Se (γ,n)^{75}Se
^{77}Br	57 h	ε, β^+	Label radiosentizers for Te quantization of hypoxia in tumors, and monoclonal antibody labeling	^{79}Br (γ,2n)^{77}Br
^{99}Mo	66 h	β^-	Parent for Tc-99m generator used for brain, liver, lungs, heart imaging	^{100}Mo (γ,n)^{99}Mo
^{131}Ba/^{131}Cs	11.5 d (9.7 d)	ε, β^+ ε	Intracavity implants for radiotherapy	^{132}Ba (γ,n)^{131}Ba ^{131}Ba (ε, β^+) ^{131}Cs
^{225}Ra/^{225}Ac	10 d	β^-, ε	Monoclonal antibody attachment used for cancer treatment (RIT), also parent of Bi-213.	^{226}Ra (γ,n)^{225}Ra ^{225}Ra (ε, β^-) ^{225}Ac

(4.5% branching ratio). A high purity germanium detector (HPGe) with 1 keV energy resolution was used to measure the count rate for the above energy lines. The measured activity of ^{99}Mo from each foil was found to be 0.9 MBq (versus the predicted value of 1.5 MBq). There are several sources of errors that may explain this discrepancy. First, the cross-section of ^{100}Mo(γ,n)^{99}Mo was approximated by the inclusive ^{100}Mo(γ,nx) cross-section (Beil et al., 1974) since an exclusive (γ,n) cross-section has not been measured experimentally. Second, the electron beam we used was not monochromatic, but had an energy spread $\Delta E/E \approx 10\%$. Finally, beam current had relatively high uncertainty of approximately 20%. With all this taken in consideration, we find agreement between the predicted and measured values of ^{99}Mo yield to be satisfactory.

The ^{99}Mo recoil energy spectrum predicted by Eq. 5 was used to calculate the distribution of ranges of ^{99}Mo ions in natural molybdenum using SRIM software (Fig. 5). As can be seen from Fig. 5, the range of a 10 keV ^{99}Mo atom in natural molybdenum is less than 5 nm and thus the size of molybdenum target particles should be of the order of nanometers. The fraction of produced ^{99}Mo ions escaping the particle was calculated as a function of the particle size. For (20 nm)^3 size particle it was found that 56% of all the produced ^{99}Mo atoms would escape the target particle. At the same, for each ^{99}Mo atom 26 ^{100}Mo atoms would escape the target as well. Stable ^{100}Mo atoms have a pronounced peak at low energies (88% of them have energy < 150 eV), while ^{99}Mo ions have a uniform distribution of energies (see Fig. 6). We have simulated different thicknesses of coating along with a few different coating materials, including Au, Cu, Al, C and SiC. The optimum size of the Mo nano-particle was found to be 20 nm. The optimum coating was found to be 5 nm carbon or silicon carbide layers (see Table 2).

This method can be applied to the production of many other isotopes. Table 3 shows some examples of medical isotopes which can be obtained via photoneutron reactions and their applications. As one can see, this is a very broad list. While commercial production of some of the isotopes with linear electron accelerators is being developed, for example ^{99}Mo (Galea et al., 2013), the majority of the isotopes from this list are not routinely produced using electron LINACs. In the case when low specific activity cannot be tolerated, kinematic recoil method could make photoneutron production of radioisotopes quite feasible.

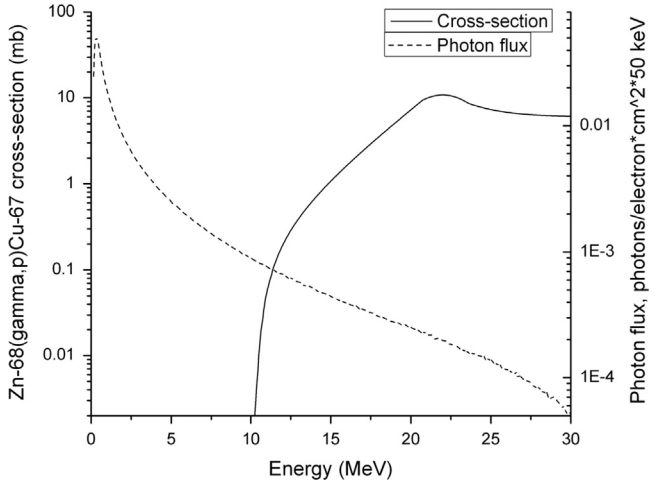

Fig. 7. ^{68}Zn(γ,p)^{67}Cu reaction cross-section (adopted from International Atomic Energy Agency (IAEA) Photonuclear Data Handbook.) and simulated average photon flux through a 40 g Zn target.

3.2. Photoproton reaction ^{68}Zn(γ,p)^{67}Cu

In the same way as we predicted ^{99}Mo activity, we have simulated photon flux through the natural Zn foils and estimated the activity of ^{67}Cu by calculating the integral of the product of photon flux and the ^{68}Zn(γ,p)^{67}Cu reaction cross-section (see Fig. 7). The activity of ^{67}Cu after 10 h of irradiation was found to be about $(0.4-1.1) \times 10^7$ Bq/(g*kW), depending on the position of the target. As one can see, this number is comparable to the (γ,n) production rate of ^{99}Mo. These simulation results were benchmarked with experimental data collected at the Idaho Accelerator Center. Table 4 summarizes the simulated and the measured activities of ^{67}Cu.

Photoproton reactions can be used to obtain a large range of medical isotopes (Table 5). Chemical separation techniques have been developed for many of them, for example to separate ^{67}Cu from ^{68}Zn a simple, reproducible and hot cell-compatible three ion-exchange matrices approach was developed (Schwarzbach, 1995). Separation techniques for other pairs, such as Hf/Lu, Zr/Y, Sn/In, etc (Le Fevre and Pin, 2005; Kandil et al., 2007).

Table 4
Simulated and measured ^{67}Cu activities as a result of natural Zn samples (thin foils) activation.

Zn sample		Foil 1	Foil 2	Foil 3	Foil 4
Distance from the converter		0.6 cm	1.1 cm	1.6 cm	2.1 cm
Activity of ^{67}Cu, MBqi/g*kW*h	Data	1.02 ± 0.04	0.64 ± 0.08	0.51 ± 0.04	0.41 ± 0.04
	Calc.	1.16	0.83	0.61	0.45

Table 5
Medical isotopes which can be obtained through the photoproton production and their possible applications.

Nuclide	Half-life	Decay mode	Possible applications	Production
^{43}K	22.2 h	β^-	Myocardium imaging	^{44}Ca (γ,p)^{43}K
^{47}Sc	3.35 d	β^-	Bone cancer pain relief, cancer radioimmunotherapy	^{48}Ti (γ,p)^{47}Sc
^{57}Co	271 d	ε	Radiolabeling agent for vitamin B12 deficiency and Schilling's test	^{58}Ni (γ,p)^{57}Co
^{67}Cu	62 h	β^-	Cancer diagnostics and radioimmunotherapy, planar imaging, SPECT imaging	^{68}Zn (γ,p)^{67}Cu
^{90}Y	64 h	β^-	Implants, radioembolization	^{91}Zr (γ,p)^{90}Y
^{111}In	2.8 d	ε	Radiolabeling Leukocytes, blood scans	^{112}Sn (γ,p)^{111}In
^{131}Ba	11.5 d	ε, β^+	Intracavity implants for radiotherapy	^{131}Ba (γ,p)^{131}Cs
^{166}Ho	26.8 h	β^-	Treatment of rheumatoid arthritis, cancer radioimmunotherapy	^{167}Er (γ,p)^{166}Ho
^{177}Lu	6.71 d	β^-	Restenosis treatment, cancer radioimmunotherapy	^{178}Hf(γ,p)^{177}Lu

4. Conclusions

The possibility of photonuclear production of Cu and Mo medical radioisotopes using linear electron accelerators was investigated. The $^{100}Mo(\gamma,n)^{99}Mo$ reaction was considered as a case study for photoneutron production. Monte-Carlo simulations were performed and the ^{99}Mo activity was predicted to be about 7 MBq/(g*kW*h). Irradiating 1 g target for 10 using 10 kW electron LINAC would result in 700 MBq. This specific activity is not enough for ^{99}Mo to be separated from ^{100}Mo using standard alumina column. However, the separation still can be done either by using low specific activity column (McAlister and Horwitz, 2009) or via kinematic recoil method described above. Photoproton production of ^{67}Cu was investigated using the reaction $^{68}Zn(\gamma,p)^{67}Cu$. The ^{67}Cu activity was predicted to be about 1 MBq/(g*kW*h). Hundreds MBq (tens of mCi) of ^{67}Cu can easily be produced on a daily basis. Several experiments were performed at the Idaho Accelerator Center using natural molybdenum and zinc foils to compare with the above predicted activities. The experimental data were consistent with the predicted values.

Acknowledgments

This research was supported by Department of Energy Grant DE-SC0002417 and by Department of Energy Grant Grant DE-SC0005749.

References

Aizatsky, N.I., Diky, N.P., Dovbnya, A.N., et al., 2010. ^{99}Mo and ^{67}Cu isotope yields under production conditions of NSC KIPT electron accelerator KUT-30. Probl. Atomic Sci. Technol. 53, 140–144.

Ball, G., 2003. Reactor calculations in aid of isotope production at SAFARI-1. J. Radioanal. Nucl. Chem. 257 (1), 65–70.

Beil, H., Bergere, R., Carlos, P., Lepretre, A., Miniac, A.D., Veyssi´ere, A., 1974. A study of the photoneutron contribution to the giant dipole resonance in doubly even Mo isotopes. Nucl. Phys. A 227 (3), 427–449.

Bokhari, T.H., Mushtaq, A., 2010. Production of low and high specific activity ^{64}Cu in a reactor. J. Radioanal. Nucl. Chem. 284, 265–271.

Cheng, K.-Y., Kunze, J.F., Ehrhardt, G.J., 1999. Investigation of recoil collection method for production of high specific activity nuclear medicine isotopes. Med. Phys. 26 (9), 1843–1846.

Danon Y., R.C. Block, R. Testa, H. Moore, Medical isotope production using A 60 MeV linear electron accelerator, NS transactions, 2008 ANS National Meeting, Anaheim, CA, vol. 98, 894–895, 2008.

Fujiwara, I, H., H., Matsumura, K. Sakamoto, et al., 1999. Recoil studies of photonuclear reactions on ^{nat}Cu, ^{nat}W,^{nat}Ta, and ^{197}Au at intermediate energies. Czechoslov. J. Phys. 49 (S1).

Galea, R., Wells, R.G., Ross, C.K., Lockwood, J., Moore, K., Harvey, J.T., Isensee, G.H., 2013. A comparison of rat SPECT images obtained using ^{99m}Tc derived from ^{99}Mo produced by an electron accelerator with that from a reactor. Phys. Med. Biol. 58, 2737–2750.

Haba, H., Matsumura, H., Miyamoto, Y., et al., 1999. Recoil properties of radionuclides formed in the photonuclear reactions on ^{nat}Cu at intermediate energies. J. Radioanal. Nucl. Chem. 239 (1), 133–138.

Haddad, F., Ferrer, L., Guertin, A., et al., 2008. ARRONAX, a high-energy and high-intensity cyclotron for nuclear medicine. Eur. J. Nucl. Med. Mol. Imaging 35, 1377–1387.

Han, H.S., Cho, W.K., Park, U.J., Hong, Y.D., Park, K.B., 2003. Current status and future plan for the production of radioisotopes using HANARO Research Reactor. J. Radioanal. Nucl. Chem. 257 (1), 47–51.

KC B., Harmon F., Starovoitova N., Stoner J., Wells D.P., Optimization of commercial scale photonuclear production of radioisotopes. In: AIP Conference Proceedings, accepted, 2012.

Kandil, S.A., Scholten, B., Saleh, Z.A., Youssef, A.M., Qaim, S.M., Coenen, H.H., 2007. A comparative study on the separation of radiozirconium via ion-exchange and solvent extraction techniques, with particular reference to the production of Zr-88 and Zr-89 in proton induced reactions on yttrium. J. Radioanal. Nucl. Chem. 274 (1), 45–52.

Kim, J.Y., Park, H., Lee, J.C., et al., 2009. A simple Cu-64 production and its application of Cu-64 ATSM. Appl. Radiat. Isot. 67 (7-8), 1190–1194.

Knapp (Russ) Jr., F.F., Mirzadeh, S., Beets, A.L., Du, M., 2005. Production of therapeutic radioisotopes in the ORNL High Flux Isotope Reactor (HFIR) for applications in nuclear medicine, oncology and interventional cardiology. J. Radioanal. Nucl. Chem. 263 (2), 503–509.

Le Bars, D., 2006. Fluorine-18 and medical imaging: radiopharmaceuticals for positron emission tomography. J. Fluor. Chem. 127 (11), 1488–1493.

Le Fevre, B., Pin, C., 2005. A straightforward separation scheme for concomitant Lu-Hf and Sm-Nd isotope ratio and isotope dilution analysis. Anal. Chim. Acta 54 (31-2), 209–221.

Maslov, O.D., Sabelnikov, A.V., Dmitriev, S.N., 2006. Preparation of ^{225}Ac by $^{226}Ra(g, n)$ photonuclear reaction on an electron accelerator, MT-25 Microtron. Radiochemistry 48, 195–197.

McAlister, D.R., Horwitz, E.P., 2009. Automated two column generator systems for medical radionuclides. Appl. Radiat. Isot. 67 (11), 1985–1991.

Mikolajczak, N., Parus, J.L., Pawlak, D., Zakrzewska, E., Michalak, W., Sasinowska, I., 2003. Reactor produced ^{177}Lu of specific activity and purity suitable for medical applications. J. Radioanal. Nucl. Chem. 257 (1), 53–57.

Sajjad, M., Lambrecht, R.M., 1993. Cyclotron production of medical radionuclides. Nucl. Instrum. Methods B79, 911–915.

Schwarzbach, R.,K.Z., 1995. Development of a simple and selective separation of ^{67}Cu from irradiated Zn for use in anitbody labeling: a comparison of methods. Appl. Radiat. Isot. 46 (5), 329–336.

Segebade, C., Weise, H.-P., Lutz, G.J., 1987. Photon Activation Analysis. Hawthorne, New York.

Starovoitova V., Foote D., Harris J. et al., Photonuclear production of medical isotopes. In: AIP Conference Proceedings, vol. 1336, pp. 502–504, 2010.

Tchelidze L., (2010) Feasibility study of accelerator based production of Mo-99/Tc-99 (Doctoral dissertation). Retrieved from ProQuest Dissertations and Theses, Dissertation number 3417887